Manuscript version: Accepted 8 May 2021
Elsevier, Surface & Coatings Technology
https://doi.org/10.1016/j.surfcoat.2021.127291

CO2 laser polishing of laser-powder bed fusion produced AlSi10Mg parts

Andrea El Hassanin[a],* , Muhannad Ahmed Obeidi[b] , Fabio Scherillo[a] , Dermot Brabazon[b]

[a] Department of Chemical, Materials and Industrial Production Engineering, University of Naples "Federico II", Piazzale Vincenzo Tecchio 80, 80125 Naples, Italy
[b] I-Form, Advanced Processing Technology Research Centre, Mechanical & Manufacturing Engineering, Dublin City University, Dublin 9, Ireland

Corresponding author. E-mail address: andrea.elhassanin@unina.it

ABSTRACT: Poor surface quality represents an important issue that needs improvement for metal Additively Manufactured parts. Both short or long wavelength lasers have been applied for surface polishing in order to improve the surface finish. In this work, the possible use of a CO2 laser for the surface polishing of AlSi10Mg parts made by Laser-based Powder Bed Fusion (L-PBF) was explored. The high surface roughness in the as-built condition can lead to increased laser energy absorption. In order to assess the effects of the main laser-related process parameters, the experiments were carried out on L-PBF samples built vertically with respect to the build platform. Their effect on the surface were evaluated by means of the surface arithmetical mean height (Sa), surface skewness (Ssk) and primary profile root mean square slope (Pdq), obtained via confocal microscopy. Micro structure evolution was also investigated by means of SEM and EDS analysis. The results showed a large reduction in surface roughness, ranging from the 67% to the 85% of the starting value. Microstructure of the remolten layer revealed an increased grain size and an increased Si content that led to an overall hardness increase from 85 to 121 HV.

Keywords: L-PBF, AlSi10Mg alloy, CO2 laser polishing, Surface roughness, SEM-EDS

Please cite this article as: Andrea El Hassanin, Muhannad Ahmed Obeidi, Fabio Scherillo, Dermot Brabazon, CO2 laser polishing of laser-powder bed fusion produced AlSi10Mg parts https://doi.org/10.1016/j.surfcoat.2021.127291

Manuscript version: Accepted 8 May 2021
Elsevier, Surface & Coatings Technology
https://doi.org/10.1016/j.surfcoat.2021.127291

1. Introduction

1.1. Powder-based metal Additive Manufacturing and surface quality

Over the last two decades, the interest in metal Additive Manufacturing (AM) processes has grown due to several benefits of these processes over traditional subtractive technologies. More specifically, the possibility to produce near-net-shape metal parts following a layer wise fashion and with a higher freedom in design is allowing applications in many industrial contexts compared, for instance, to conventional CNC machining [1]. Moreover, the increasing availability of different metal and alloy feedstock suitable for AM provides a further boost to the already widespread use of this manufacturing process [2]. Powder-based metal AM processes such as Laser Powder Bed Fusion (LPBF), Electron Beam Powder Bed Fusion (E-PBF) and Laser Metal Deposition (LMD) represent the leading technologies for the metal additive manufacturing of parts. These technologies provide at the same time a more efficient use of raw materials and a part building rate that is independent from the degree of part design complexity [1]. On the other hand, the current lack of a deep know-how combined with some intrinsic characteristics of these processes results in several drawbacks such as entrained porosity, high residual stresses and poor surface quality [3]. Concerning the latter, it is well established that metal AM produced parts have a high surface roughness (often identified as the profile arithmetic height distribution, Ra [4]), ranging from few to several tens of micron depending on the specific case [5]. This level of roughness makes such parts unacceptable for many end use applications. The fundamental mechanisms that contribute to this issue are also well described in the literature, namely the powder particle size distribution, the laser spot size, the staircase effect and the balling effect. These lead to a rough surface texture characterized by the presence of visible overlapped layers and sintered metal powders [3,6]. These aspects continue to be issues, despite the work on process parameter optimization and the adoption of what are called in-situ contour strategies [1,7]. This makes necessary in many cases therefore the adoption of a post process surface finishing step in order to improve the surface quality of the manufactured parts and to meet the required final surface roughness.

1.2. Post-process surface finishing techniques for metal additively manufactured parts

According to the state of the art, surface roughness of metal AM parts can be reduced by means of different techniques that can be classified according to the interaction nature with the surface, i.e. mechanical, chemical/electrochemical and thermal. Given the large number of those techniques, some authors proposed a comprehensive review work in this context [8,9].

Mechanical interaction-based treatments mainly include CNC machining [10,11], shot peening [12,13], vibratory polishing, sand blasting [14,15] and so on. Moreover, other technologies typically used in other contexts were subjected to a feasibility study in the surface finishing context, given their higher capability of access into complex parts features in comparison with the previously mentioned techniques. Examples of these processes are the Fluidized Bed and Hydrodynamic cavitation technologies [16–19]. However, in general, mechanical based surface treatments present strong limitations related to the physical access of tools and abrasive media into complex parts shapes such as the ones achievable with AM.

Chemical and electrochemical-based surface treatments, on the other hand, have the advantage of the higher mobility of the chemically aggressive solutions employed in comparison to abrasive media and machining tools, making therefore these treatments very suitable for high complex parts. Moreover, the presence of an electric potential improves the not close control of the material removal rate [20], probably the main drawback of pure chemical interaction-based finishing processes. In literature, those treatments are often called Chemical polishing

Manuscript version: Accepted 8 May 2021
Elsevier, Surface & Coatings Technology
https://doi.org/10.1016/j.surfcoat.2021.127291
and Electro polishing, according to the work of several authors conducted on parts produced by L-PBF and E-PBF technologies [21–23]. It is worth to mention that and both Chemical polishing and Electro polishing are capable to perform a selective material dissolution with respect to the surface asperities. In Chemical polishing, higher etching rates can be achieved on the surface peaks against the valleys if the chemical solutions are properly conceived. This effect is also quite useful for the removal of the molten pool edges underlying the sintered powders-rich texture of powder-based metal AM parts. On the other hand, the surface symmetry improvement can be enhanced in Electro polishing due to greater etching rates for the surface peaks imposed by the electric potential.

Thermal interaction-based finishing processes consist in providing a certain heat input on the surface, in order to promote its smoothing through different surface modification mechanisms such as re-melting and ablation [24]. Laser polishing represents in this scenario one of the main investigated finishing processes. Despite similar considerations to mechanical finishing processes are also valid in this case such as the limited physical access into complex part features, laser polishing offers several advantages such as very precise control of the process parameters, high level of process automation and a very high surface quality. Moreover, the thermal cycles imposed by laser polishing determines a superficial microstructure refinement, enhancing properties such as corrosion and wear resistance. In this scenario, several authors have investigated the effects of laser polishing on the surface quality of metal AM parts. This work has mostly been performed for the L-PBF process and both in-situ and ex-situ approaches have been investigated for several alloys such as aluminum [25,26], stainless steel [27,28] and titanium alloys [29]. The majority of the provided contributions have been related to the use of fibre laser, such as Neodymium-doped Yttrium Aluminum Garnet (NdYAG) and Ytterbium (Yb) sources. The latter laser type also represents the most utilized laser in L-PBF machines. The relatively short wavelength (1.07 μm) of the fibre lasers compared to that of the CO2 laser (10.6 μm) enables better energy absorption. The lower wavelength is more typically highly absorbed by most of the metals and alloys, for which the CO2 laser wavelength is relatively poorly absorbed [30], especially for high reflective metals such as aluminum and copper. This aspect was further demonstrated by the recent yet poorly explored research trend in the context of laser pol ishing, related to the use of pulsed lasers with an ultrashort pulse duration that guarantees a very high radiation absorption as well as a high retaining of the microstructure features [31]. On the other hand, it is also well known that the laser radiation absorption mechanisms do not depend solely from the material itself, but also from the surface roughness. If the latter is greater than the laser wavelength, the absorption mechanisms are also dictated from optical considerations such as multiple reflections of the laser beam within the surface asperities [24]. Taking in consideration that the typical surface roughness range of the as-built L-PBF parts is 6–25 μm [5], the aforementioned roughnessinduced laser absorption enhancement could extend the use of the more widely available and employed CO2 laser [28,32–34] also for the polishing of the aforementioned high reflective materials. With this premise, this work investigated the possibility to employ a CO2 laser to perform ex-situ surface polishing of L-PBF parts made with AlSi10Mg alloy, the latter widely used in aerospace and automotive parts applications. More specifically, the following questions were arisen and answered, assumed that CO2 laser is less absorbed than fibre laser but it provides higher output power and it is still the most used laser type for a large number of applications: (i) Is it possible to perform a satisfactory polishing process by taking advantage of the undesired rough surface of the as-built AM parts for an enhanced laser absorption? (ii) If so, which is the effect of the laser power, scanning speed, overlap between the tracks and focus position on the surface texture and microstructure evolution of the considered samples?

Manuscript version: Accepted 8 May 2021
Elsevier, Surface & Coatings Technology
https://doi.org/10.1016/j.surfcoat.2021.127291

2. Materials and methods

2.1. L-PBF samples

The experiments were carried out on square flat samples (dimensions: 20 × 20 × 2 mm3), built by means of L-PBF with a vertical build orientation, see Fig. 1(a). AlSi10Mg powders provided by EOS GmbH were used as the feedstock, with D10, D50 and D90 of 13.3 μm, 31.2 μm and 56.8 μm respectively. Fig. 1(b) shows an SEM image of the AlSi10Mg powders employed. The samples were manufactured by means of an EOS EOSINT M280 L-PBF machine (no longer in production), and the process parameters used to produce the samples were related to the locked exposure profile EOS Part Property Profile AlSi10Mg Speed 30 μm provided by EOS GmbH. The printing parameters were set to: beam power P = 370 W, hatch distance h = 0.19 mm and scanning speed v = 1300 mm/s. A layer thickness of 30 μm was used resulting in a volumetric energy density VEDH = 49.9 J/mm3. The scan strategy was stripes, rotated at each layer by an angle of 67◦in order to homogenize the heat distribution, according to the aforementioned EOS process parameters profile. The produced L-PBF samples were subsequently stress relieved at 300 ◦C for 2 h.

2.2. CO2 laser polishing

2.2.1. Experimental setup

The CO2 laser polishing experiments were carried out by means of a Rofin DC-015 CO2 laser, whose technical specifications are reported in Table 1 [35]. Fig. 2a presents a scheme of the experimental setup used. The samples were clamped on a steel vise mounted on the translation stage of the laser machine and supported beneath with an aluminum back-plate. The latter was used in order to avoid distortions of the sample subjected to the heat input, by the efficient dissipation of the generated heat. Fig. 2b illustrates the raster- polishing strategy adopted for the experiments, having a total laser polish width of 10 mm.

2.2.2. Experimental campaign

In order to roughly identify the process parameters with the most significant effect on the surface texture evolution and their levels, a few preliminary tests were initially considered including laser power, scanning speed and the percentage overlap between adjacent tracks. Subsequently, a 33 full factorial Design of Experiments (DoE) was carried out with the laser power (P), the scanning speed (V) and the percentage overlap between two adjacent polishing tracks (OV%). In these experiments, the laser focus position was fixed and set on the peaks of the surface and the argon shielding gas pressure which was set at 0.2 bar. Table 2 lists the levels of the process parameters investigated for the DoE, while Table 3 reports the conditions for all the 27 experiments, each of them carried out three times in order to evaluate the repeatability of the results. Table 3 reports also the corresponding values of the energy input per unit area E (J/mm^2), calculated according to the following Eq. (1) [36]:

$$E = \frac{P}{2r_b V} \quad (1)$$

where P represents the laser power provided (W), 2rb represents the laser spot diameter (mm) and V represents the laser scanning speed (mm/min). The OV% values noted were achieved with the corresponding hatch spacing noted in Table 2 for the spot size of 200 μm.

Manuscript version: Accepted 8 May 2021
Elsevier, Surface & Coatings Technology
https://doi.org/10.1016/j.surfcoat.2021.127291

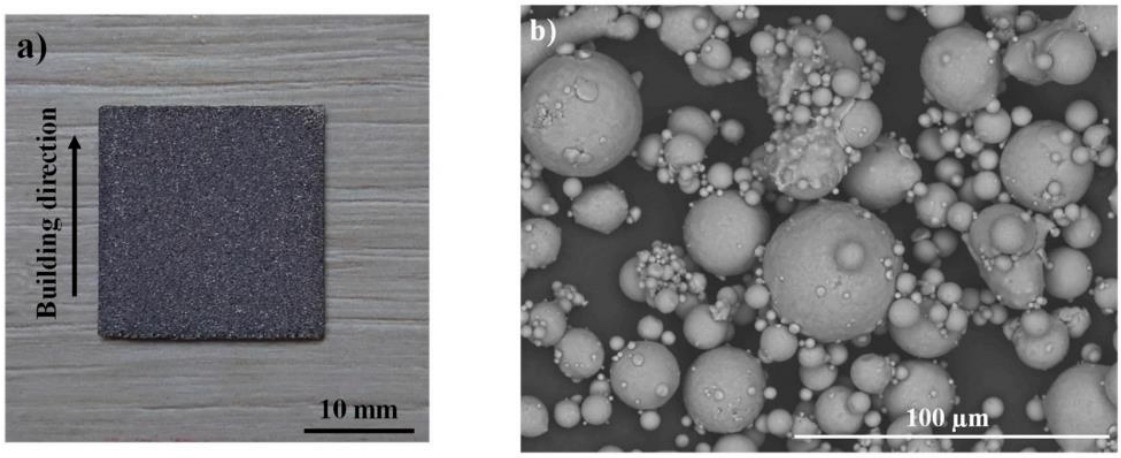

Fig. 1. (a) Picture of the L-PBF produced sample, and (b) SEM image of the AlSi10Mg powder feedstock (magnification 1000×).

Table 1
Technical specifications of the Rofin DC-012 CO_2 laser [35].

Source wavelength (λ)	10.6 µm
Beam quality factor (M^2)	1.05
Max. power	1.5 kW
Focus diameter	200 µm
Laser mode	Continuous wave
x-y stage speed	0 to 5000 mm/min
Shielding gas	Argon

Based on the best process conditions obtained from the DoE, the influence of the laser focus position with respect to the surface was also investigated. In this case, the aim of the tests was to evaluate the effect of the focus shift above the surface peaks, in order to provide a range of experimental energy density inputs on the surface. The defocused beam experiments were carried out considering a total focus shift of 3 mm, taking as a reference the focal position used for the DoE experiments, and the effect of this process variable was investigated considering three steps in level each consecutive being set 1 mm further apart from the other. Moreover, in order to quantify E in this process configuration, the new theoretical values of the laser spot for each defocusing condition were calculated according to the Eq. (2), applicable only for the Gaussian CO2 laser beam [37]:

$$r = r_f \sqrt{\left[1 + \left(\frac{\lambda z}{\pi r_f^2}\right)^2\right]} \qquad (2)$$

where r represents the new value of the beam spot radius (µm), rf is the radius of the laser focus (µm), λ is the laser wavelength (µm) and z is the distance of the laser focus from the surface (µm). The calculated spot values were also used to quantify the new values of E, after having fixed the best values of P and V from the DoE experiments. Moreover, as for the DoE experiments, each experiment in the defocused beam condition was carried out three times to evaluate the repeatability of the results.

Manuscript version: Accepted 8 May 2021
Elsevier, Surface & Coatings Technology
https://doi.org/10.1016/j.surfcoat.2021.127291

Table 2
Factors and levels considered for the DoE experiments.

	Power (W)	Scanning speed (mm/min)	OV %	Hatch (μm)
Level 1	350	500	50	100
Level 2	450	750	65	70
Level 3	550	1000	80	40

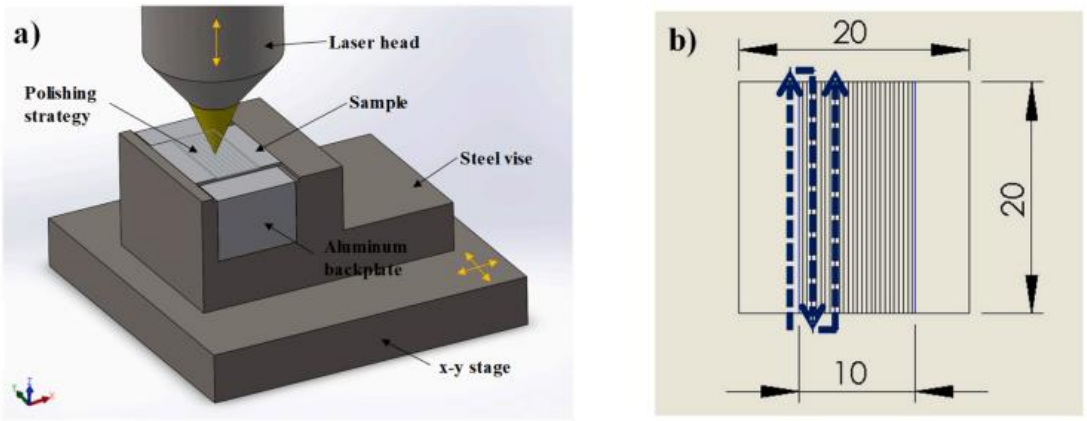

Fig. 2. (a) General scheme of the CO2 laser polishing experimental setup and (b) illustration of the adopted polishing scan strategy.

Table 3
Experimental combinations of the DoE experiments.

Run	P (W)	V (mm/min)	OV%	E (J/mm^2)
1	550	750	50	220
2	450	500	80	270
3	550	750	80	220
4	550	500	65	330
5	350	1000	50	105
6	450	1000	50	135
7	550	1000	80	165
8	450	500	65	270
9	350	1000	65	105
10	550	500	80	330
11	550	1000	50	165
12	450	750	50	180
13	350	750	80	140
14	350	500	80	210
15	350	750	65	140
16	450	750	65	180
17	450	1000	80	135
18	450	750	80	180
19	450	1000	65	135
20	550	1000	65	165
21	350	500	65	210
22	350	500	50	210
23	450	500	50	270
24	350	750	50	140
25	350	1000	80	105
26	550	500	50	330
27	550	750	65	220

Manuscript version: Accepted 8 May 2021
Elsevier, Surface & Coatings Technology
https://doi.org/10.1016/j.surfcoat.2021.127291

2.2.3. Characterization procedure

Before and after the treatment, the samples were cleaned in a distilled water ultrasonic bath for 15 min, and then dried at 80◦C for 1 h. Subsequently, the results in terms of surface modification were analyzed with a Leica DCM3D confocal microscope. Confocal microscopy is a flexible surface characterization technique, provides reliable results compared to stylus profilometry, and provides the possibility to analyze both areal and profile surface roughness parameters [38]. For each sample, an 8 × 8 mm2 area was considered in order to acquire a consistent region of the sample without edge effects and using the sample center as the reference point. The acquired surfaces were then corrected for tilt, shape and missing points errors before extracting the surface texture parameters by means of the in-bundle software Leica Map® v7. Given the random texture of the L-PBF process resulting surface, no filtering operations were considered. Concerning the surface texture parameters, the surface arithmetical mean height Sa and the surface skewness Ssk were investigated as areal parameters [39]. The former represents the areal equivalent of the most widespread Ra, whereas the latter describes the distribution symmetry of the peaks and the valleys within the acquired area. The results were plotted considering the average and the standard deviation calculated on the basis of the three experiments carried out for each set of processing conditions. The root mean square slope of the primary profiles, Pdq, was calculated in order to evaluate the steepness of the surface [40,41]. According to literature [42], this parameter is related to the smoothness and brilliance of a surface. Moreover, in the specific context of this work, Pdq could represent a further useful indicator of the smoothing mechanisms in relation to the specific surface texture investigated for the as-built samples. On the other hand, the equivalent areal parameter, Sdq, was not investigated since it describes a surface gradient that evaluates the shape evolution rather than the asperities [39]. The Pdq values reported in this work were calculated on the basis of ten profile measurements, five for each of the two principle laser processing directions, and then averaged for both the profile measurements and repeatability. The profiles were directly extracted from the acquired areas, using the profile extraction function included in Leica Map® v7. To better understand the results obtained from confocal microscopy, a qualitative analysis of the treated surfaces was carried out by performing in-plane imaging with an Hitachi TM3000 SEM.For the qualitative comparison, 3D surface plots obtained from confocal microscopy were also considered, showing the heights distribution in color-coded scale and reporting a histogram that indicates the mean height distribution of the topo graphical events (the peaks or the valleys). The images were taken in order to compare the surface morphology before and after polishing. Moreover, a detailed metallography analysis was carried out to inves tigate the microstructure evolution. The samples investigated in this case were those that produced the lowest and highest surface roughness results for the DoE experiments, and the samples treated with the different defocused beam conditions. After metallographic specimens preparation [43], the microstructure analysis was carried out first from the observation of optical macrographs obtained by means of a Zeiss Axioplan 2 Optical Microscope. To prepare the samples for metallography, they were cut perpendicularly to the polishing tracks and then etched by swabbing the surface for 10s with a 0.2% vol HF aqueous solution. The macrographs were analyzed to reveal the molten pools derived from the laser polishing and to measure the laser polishing resulting melt pool depth. Subsequently, SEM analysis was also carried out on the same sections to evaluate qualitatively the microstructure evolution from the comparison of the grain morphology between the molten and the base material under the different treatment conditions. Moreover, Energy Dispersive X-ray Spectroscopy (EDS) analysis was adopted to evaluate the chemical composition changes experienced from the material during polishing, using a SwiftED 3000 EDS probe integrated in the SEM.

Manuscript version: Accepted 8 May 2021
Elsevier, Surface & Coatings Technology
https://doi.org/10.1016/j.surfcoat.2021.127291

3. Results

3.1. Design of experiments results

Fig. 3 shows the evolution of Sa before and after the treatment, as a function of E and OV%. For the sake of brevity, the evolution of Ssk and Pdq is reported in Table 4. Before polishing, the L-PBF samples had Sa values mostly above 20 μm and with considerable variability relative to the laser polished samples. The resulting Sa values after the laser polishing shows that every investigated polishing condition led to a significant roughness reduction. An increase of both E and OV% led to a reduction in Sa. The best case observed within the DoE process window was obtained by the combination of highest values of E (330 J/mm^2) and OV% (80%), and lowest scan speed. This process parameters led to a Sa of 7.9 ± 0.8 μm, Run 10 from Table 3. Excessive energy density and overlap could lead to excessive surface melting and hence to an increased surface roughness. However, it is clear that this was not the case within the process parameter range investigated. While the resulting average Ssk values were higher for the non-laser polished samples, no clear trends can be observed even after polishing. A much higher level of surface roughness was again detected for the non-treated samples. On the other hand, the negative Ssk values suggest that the surfaces of the as-built samples are asymmetrical from the valleys side, whereas the polishing treatment promoted an increase of this asymmetry, i.e. exerting a prevalent smoothing effect on the surface peaks (for the best case, the measured final value was − 0.1 ± 0.2, which is close to zero that represents the ideal symmetry condition). Concerning the evolution of Pdq, a very similar trend to Sa can be observed according to the data reported in Table 4. Also in this case, the highest reductions were measured for Run 10 with a measured final value of 6.1 ± 1.7◦.

Table 4
Surface texture parameters comparison before and after the DoE tests.

Run	S_a (μm)		S_a st.dev. (σ) (μm)		S_{sk}		S_{sk} st.dev. (σ)		P_{dq} (°)		P_{dq} st.dev (σ) (°)	
	Before	After	Before	After	Before	After	Before	After	Before	After	Before	After
1	23.2	10	0.9	0.7	−0.2	−0.3	0.2	0.3	48.4	10.1	3.8	0.5
2	22.5	10.0	2.4	0.2	−0.1	−0.4	0.5	0.4	45.3	8.2	8.9	0.2
3	21.6	8.7	1.3	0.7	−0.2	−0.7	0.4	0.5	44.3	7.6	9.3	1.6
4	20.6	10.5	3.1	1.6	−0.3	−0.3	0.4	0.1	47.6	6.3	4.2	0.9
5	20.2	13.6	0.8	1.2	−0.1	−0.4	0.1	0.1	49.8	13.8	4.3	1.5
6	21.5	10.6	0.9	0.5	−0.1	−0.3	0.0	0.2	45.3	11.6	5.1	0.7
7	21.4	9.3	1.1	0.2	−0.1	0.2	0.3	0.5	47.4	6.2	4.5	2.1
8	24.7	10.5	3.0	0.2	0.0	−0.3	0.1	0.4	48.1	9.7	6.6	0.6
9	20.9	11.7	0.1	0.1	−0.2	−0.4	0.1	0.0	43.7	12.0	5.7	1.6
10	22.3	7.9	1.3	0.8	−0.1	−0.1	0.4	0.2	42.2	6.1	9.0	1.7
11	19.6	9.7	2.0	1.0	−0.3	−0.7	0.3	0.9	41.6	9.2	7.6	2.3
12	22.5	10.2	1.2	0.6	0.0	−0.2	0.2	0.3	44.9	9.6	7.0	1.5
13	22.0	10.7	1.0	1.0	−0.1	−0.6	0.4	0.1	43.4	7.9	11.9	1.9
14	21.6	10.0	1.0	1.2	−0.3	−0.4	0.1	0.2	42.2	6.4	6.8	2.0
15	22.4	11.7	2.1	0.6	−0.3	−0.5	0.2	0.0	48.1	11.8	5.5	1.1
16	22.1	10.8	1.8	1.6	−0.6	−0.3	0.3	0.1	42.5	9.2	7.9	1.0
17	21.8	9.3	1.0	0.3	0.0	−0.5	0.2	0.2	44.7	8.1	4.1	0.6
18	22.6	8.7	0.8	1.1	0.1	−0.5	0.1	0.1	48.1	7.0	6.7	1.4
19	22.4	10	1.0	0.4	−0.3	−0.3	0.3	0.2	44.2	9.4	8.3	0.6
20	20.2	9.1	1.2	0.7	0.1	−0.3	0.5	0.0	41.3	8.2	6.7	0.6
21	21.0	10.3	1.7	0.5	−0.2	−0.4	0.2	0.1	44.6	11.0	4.6	1.4
22	22.1	11.2	2.2	0.3	0.0	−0.6	0.4	0.2	45.8	10.2	9.1	1.0
23	20.7	10.4	0.6	0.3	0.2	−0.3	0.2	0.1	43.0	9.6	4.5	2.6
24	21.9	12.1	3.1	0.6	−0.1	−0.3	0.7	0.1	43.6	11.6	8.3	2.4
25	21.2	10.9	0.9	0.5	0.0	−0.4	0.3	0.1	42.5	9.1	10.3	1.5
26	22.1	9.1	2.4	0.9	−0.4	−0.4	0.3	1.0	44.3	5.0	10.8	0.1
27	22.4	8.9	0.6	0.8	−0.2	−0.3	0.2	0.4	43.9	5.8	8.7	1.4

The effect of the different polishing conditions in comparison with an as-built surface can be also observed from the 3D plots depicted in Fig. 4, reporting the acquired surfaces of the worst (Run 5) and the best (Run 10) laser polishing cases.

The quantitative results observed were supported by the in-plane SEM observation of the samples. Fig. 5 shows the SEM images of the not treated surface, and the treated surfaces of Run 5 (highest roughness resulting from the lowest E and OV%, see Table 3) and Run 10 (lowest roughness resulting from the highest E and OV%, see Table 3). Expectedly, the as-

Manuscript version: Accepted 8 May 2021
Elsevier, Surface & Coatings Technology
https://doi.org/10.1016/j.surfcoat.2021.127291

built surface presents a sintered powder-rich texture and some crater-like defects generated during the L-PBF process. On the other hand, there was no evidence of residual sintered powder for the lowest surface roughness condition, which was found for Run 10. Concerning the worst laser polish case of Run 5, the SEM image shown in Fig. 5 presents regularly repeating regions of lack of melting (dark lines) and higher levels of melting. To explain this, it could be considered that as the focused laser is scanned across the surface and taking the temperature at the center of the laser spot, a temporal temperature profile along the laser track path is created which is not constant but rather is uniformly repeating, thus causing increases and decreases of the temperature along the scan track. The corresponding peaks and trough regions would then correspond to where there is more and less molten and solidified material as is observed in the direction of the laser scan itself. Moreover, the differences in terms of surface modification between the worst and best laser polish scenarios are also clearly visible from the optical macrographs reported in Fig. 6, obtained from the crosssectional microstructure observation. Concerning the not treated surface, the macrograph revealed the typical defects of the L-PBF process, such as gas inclusions and lack of melting within the material, and the sintered powders on the surface due to the balling effect. On the other hand, the worst case surface morphology appears more wavy with more pronounced higher depth region with asperities and a lower depth region. Moreover, the overall average re-melting depth was less for Run 5 (84 ± 13.3 μm) compared to Run 10 (115 ± 11.3 μm). For both Run 5 and 10, the resulting molten pools can be clearly seen in the polished zone (PZ), overlapping the preexisting ones produced from the L-PBF process. Furthermore, a heat affected zone (HAZ) can be clearly seen at the interface between the base material (BM) and the PZ, as well as at the interface between the produced molten pools.

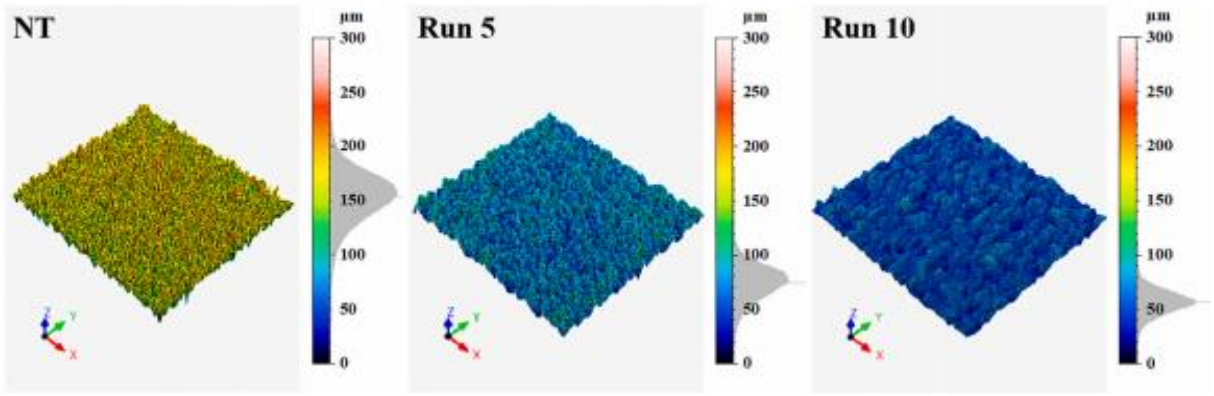

Fig. 4. Comparison between the 3D surfaces, obtained through confocal microscopy, of the not treated surface (NT), the worst polishing case (Run 5) and the best polishing case (Run 10).

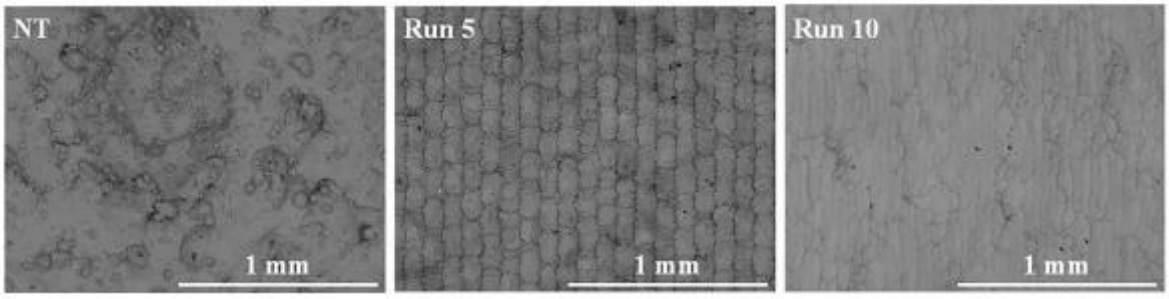

Fig. 5. SEM images for the top view comparison between the not treated surface (NT), the worst polishing case (Run 5) and the best polishing case (Run 10) (100× magnification).

Manuscript version: Accepted 8 May 2021
Elsevier, Surface & Coatings Technology
https://doi.org/10.1016/j.surfcoat.2021.127291

In order to provide a more detailed microstructure description, Fig. 7 shows the SEM images of the main microstructure features observed above. Given the primary importance of the surface quality improvement, this observation is reported for sake of brevity only for Run 10. In the BM region (Fig. 7a), the typical microstructure of the L-PBF processed AlSi10Mg was observed, i.e. a very fine cellular microstructure composed by Al grains surrounded by a Si-rich eutectic phase [44]. In the HAZ (Fig. 7b), a coarsening of the Al grains and an alignment towards the laser axis direction can be noted. Moreover, the thickness of the eutectic phase increased, as shown in the PZ (Fig. 7c) and in the latter the grains appear to be more equiaxed.

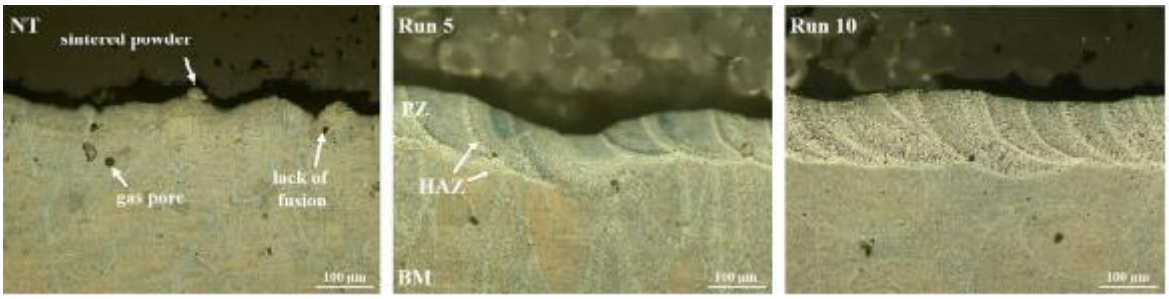

Fig. 6. Cross-sectional view of the optical macrographs showing the morphology and microstructure comparison between a not treated surface (NT), the worst (Run 5) and the best (Run 10) DoE resulting roughness levels (BM = base material; HAZ = heat affected zone; PZ = polished zone; 100× magnification).

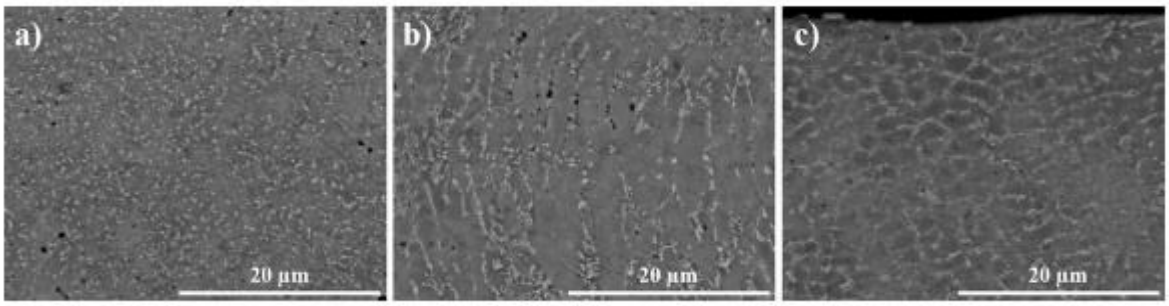

Fig. 7. High magnification SEM images of the microstructures observed in the different regions for Run 10: a) BM, b) HAZ and c) PZ (5000× magnification).

3.2. Defocused laser beam experiments results

According to the previous results, the process parameters related to the Run 10 experiment were identified as the best (P = 550 W; V = 500 mm/min; OV% = 80). Therefore, having fixed this process parameters set, Fig. 8 reports the Sa evolution as a function of the laser focus position shifts of 1, 2, and 3 mm above the surface. More specifically, the comparison between Run 10 for the different laser focal positions is reported. As for the DoE experiments, the evolution of all the investigated surface texture parameters is reported in Table 5 and 3D surface plots are also reported in Fig. 9. Despite the high uncertainty of the values before the treatment, the Sa evolution reported in Fig. 8 indicates a clear decreasing trend for Sa with an increase in the distance of the focal plane from the surface. Moreover, when the focus was set 3 mm above the surface peaks, the largest reduction is Sa was observed, with a final Sa value of 3.3 ± 1.3 µm. Nonetheless, a reduction in Sa over that of the focal position on the surface was also observed with the +1 and + 2 mm focus shift conditions, as reported in Fig. 9. Concerning the Ssk evolution, a more clear trend was observed compared to the DoE experimental results. More specifically, the results suggest that the surface symmetry is more

Manuscript version: Accepted 8 May 2021
Elsevier, Surface & Coatings Technology
https://doi.org/10.1016/j.surfcoat.2021.127291
close to an equal distribution of residual peaks and valleys after polishing, since the skewness approached to zero for each investigated condition. However, given the significant uncertainty, this conclusion cannot be drawn with a high degree of confidence. On the other hand, the evolution of Pdq revealed a relative independence of this parameter from the laser focus position, considering the very small differences measured: even for the best case observed in terms of Sa (Run 10 F + 3), the final Pdq value of 5 ± 1.7◦ is slightly different from the ones measured for Run 10 and for the other defocused beam conditions. All these considerations were supported again by the in-plane SEM observations reported in Fig. 10, from which an increase of treated surface flatness was observed as a function of the laser focus shift increase.

The transverse microstructure evolution is reported in Fig. 11. Besides the presence of the same microstructure features observed for the DoE experiments, the observations revealed in this case an increase of the re-melting depth in comparison with Run 10 (115 ± 11.3 μm against 132 ± 8.5 μm for Run 10 F + 1, 191 ± 8.2 μm for Run 10 F + 2 and 222 ± 5.4 μm for Run 10 F + 3) as well as the presence of more porosities, mostly located towards the bottom of the PZ. The macrographs revealed also that the porosity level increased with the increase of the laser focus shift. As for the DoE experiments, a detailed microstructure observation by means of SEM is reported in Fig. 12, for sake of brevity only for the defocused beam condition that provided the best surface quality improvements (Run 10 F + 3). The results showed that the microstructure alterations occurred are very similar to the ones observed for Run 10 (see Fig. 7).

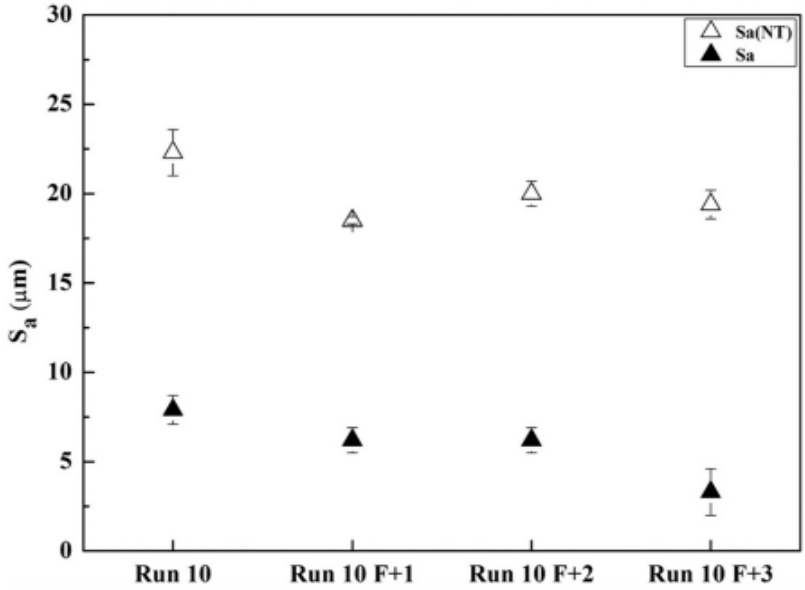

Fig. 8. Sa comparison before and after the defocused beam experiments (NT = not treated); whiskers about the mean points represent ± one standard deviation.

4. Discussion

4.1. Surface texture evolution

The first result observed concerning the surfaces of the as-built samples produced in this study was the higher variability of the surface for the L-PBF process compared to the laser polished surface roughness. As a general consideration, roughness result variability can be ascribed to the well-known balling effect occurring during L-PBF process, whereas the stair-step effect contribution was negligible given the geometry and the building direction used for the samples. Another LPBF process variable that has to be considered as a source of the surface quality variance is the size distribution of the powders feedstock. More specifically, a highly dispersed powder particle size distribution promotes a less efficient powder settling on the build platform

as well as the formation of asperities of different heights, i.e. more loosely sintered powders. It is also worth to note that the latter contributes also to the formation of undercuts and crater-like defects (see Fig. 6), which are difficult or even impossible to be acquired with confocal microscopy.

An important outcome of the presented experimental work was that the process parameters combination related to the highest value of E, derived from the highest P and the lowest V, resulted in the lowest level of roughness within the DoE tests, as shown in Fig. 3 and Table 4. Despite the fact that, in general, more consistent surface modifications with higher energy inputs are expected, it can be considered in this case that the higher energy density input, with the more absorbing rough LPBF produced surface, compensated for the generally otherwise poor absorption of CO2 laser by AlSi10Mg. Given the Gaussian distribution of the laser beam, the higher OV% also provided better uniformity in surface energy exposure and hence melt pool layer thickness uniformity. It was observed that if an insufficient value of OV% was provided as well as an insufficient energy input, a wavy surface was generated after laser polishing. The latter observation was supported in first instance from the evolution of Ssk reported in Table 4, the in-plane SEM observations reported in Fig. 5 and the surface morphology comparison between Run 5 and Run 10 through the 3D surfaces and optical macrographs illustrated in Figs. 4 and 6.

Table 5
Surface texture parameters comparison before and after the defocused beam experiments.

Run	S_a (μm)		S_a st.dev. (σ) (μm)		S_{sk}		S_{sk} st.dev. (σ)		P_{dq} (°)		P_{dq} st.dev (σ) (°)	
	Before	After	Before	After	Before	After	Before	After	Before	After	Before	After
10	22.3	7.9	1.3	0.8	−0.1	−0.1	0.4	0.2	42.2	6.1	9.0	1.7
10 F + 1	18.5	6.2	0.2	0.7	−0.3	−0.1	0.1	0.1	41.3	4.6	7.1	1.5
10 F + 2	20	6.2	0.7	0.7	−0.3	−0.1	0.2	0.2	44	5.6	11	0.4
10 F + 3	19.4	3.3	0.8	1.3	0.3	0.2	0.3	0.2	49	5	5.3	1.7

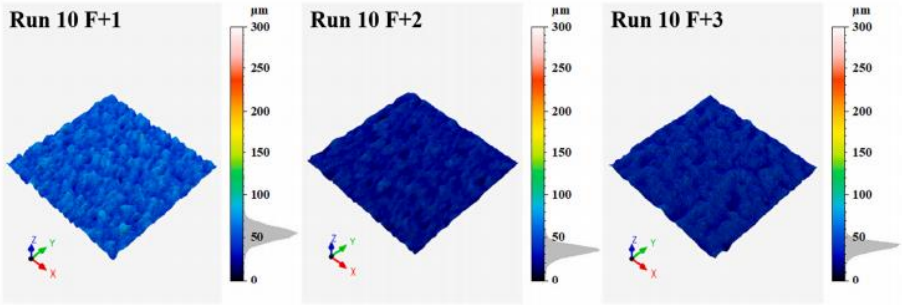

Fig. 9. Comparison between the 3D surfaces, obtained through confocal microscopy, of the laser polished samples with the different defocused beam conditions.

Furthermore, in relation to the Pdq evolution reported in Table 4, the general outcome is that this parameter is strictly related to the sintered powders on the L-PBF as-built surface. More specifically, it can be observed that the main contribution of the profiles steepness is given by the sintered powders, whose removal after polishing provides a significant Pdq reduction, as similarly observed for Sa. Therefore, according to the observed trends, the sintered powders layer removal represents therefore a primary surface modification mechanism, taking place due to surface re-melting. This is also supported by the presence of the observed new molten pools, see Figs. 6 and 11, as well as from the negligible average weight variation measured for the samples before (2.0887 ± 0.0085 g) and after (2.0871 ± 0.0091 g) the treatment. Moreover,

Manuscript version: Accepted 8 May 2021
Elsevier, Surface & Coatings Technology
https://doi.org/10.1016/j.surfcoat.2021.127291

concerning the investigated process parameters, it can be concluded also that the OV% has a prevalent effect on Pdq compared to P and V.

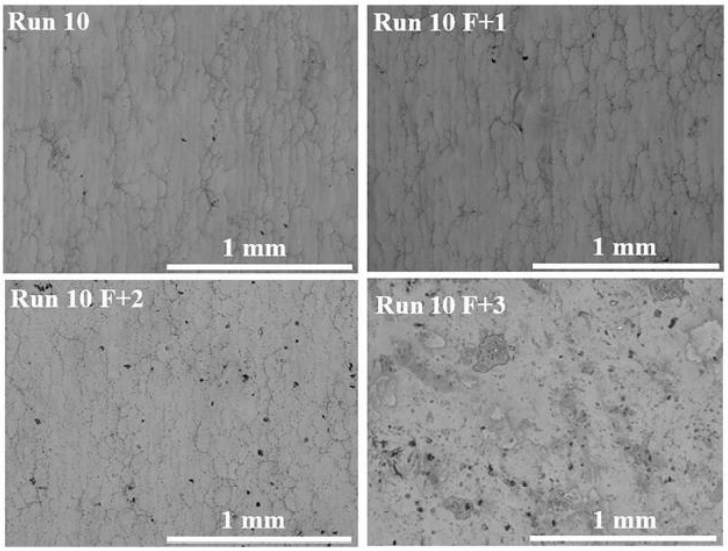

Fig. 10. Top-view SEM images comparison between the DoE experiment (Run10) and the three investigated defocused beam conditions (100× magnification).

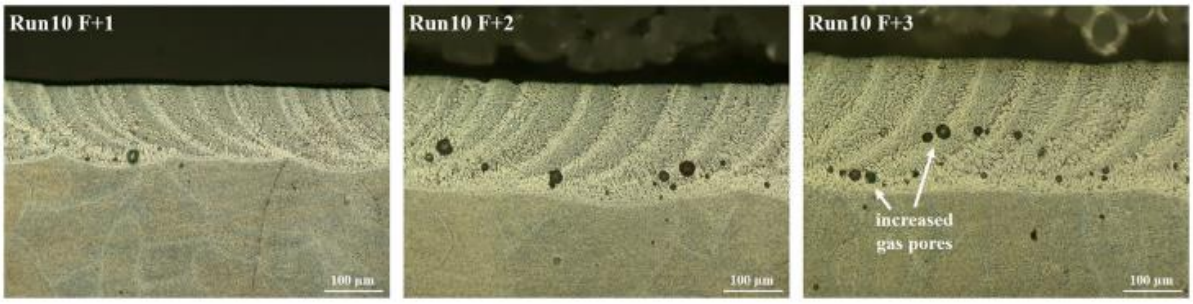

Fig. 11. In-section optical macrographs showing the morphology and microstructure comparison between the samples treated with the three different defocused beam conditions (100× magnification).

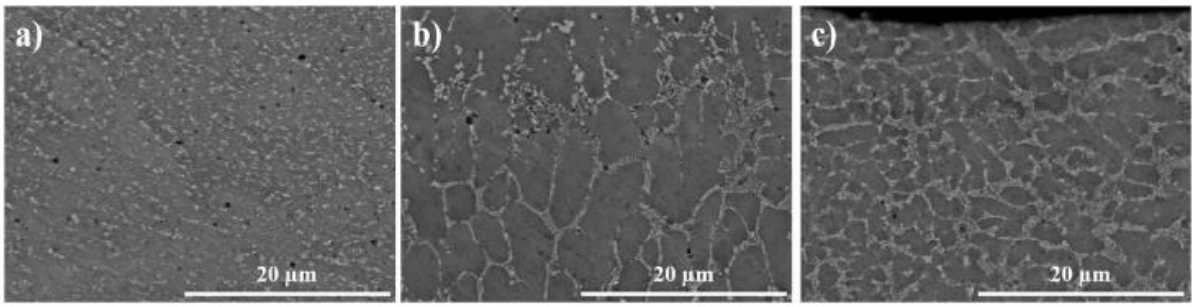

Fig. 12. High magnification SEM images of the microstructures observed in the different regions for the best case of the defocused beam experiments (Run 10 F + 3): a) base material, b) HAZ and c) polished zone, (5000× magnification).

From the analysis of the subsequent defocused beam experiments, the results revealed that the laser focus position set above the surface provided a significant improvement in the surface quality, where all the other process parameters were fixed from the DoE for the case, Run 10. However, this result is most likely ascribed to the further OV% increase dictated by the laser

Manuscript version: Accepted 8 May 2021
Elsevier, Surface & Coatings Technology
https://doi.org/10.1016/j.surfcoat.2021.127291
focus shift, despite the original value fixed at 80%. To better discuss this aspect, in Table 6 are reported the theoretical values of the laser spot calculated using Eq. (2), based on the three investigated focal positions. The determined values were used also to calculate the corresponding new values of E and OV%, the latter based on geometric considerations between two overlapping laser spots with the same hatch spacing as set for the 80% OV spot surface focus condition. From the obtained results it can be concluded that the OV% increase compensates the lower E values in relation to the surface modification. More precisely, the OV% increase provides exposure of a same surface region to a discrete number of thermal cycles. With this premise, the defocused beam condition led to a higher heat input on a considered surface region, due to a more prolonged residence time of the beam due to the OV% increase. This observation was supported by the increase of the measured re-melting depth, as also reported in Fig. 11.

Other factors might have contributed to the surface finish improvements observed in the defocused beam experiments. In first instance, the aforementioned OV% increase subsequent to the laser focus shift determined a greater compensation of the differential polishing effects due to the Gaussian distribution of the laser, as well as a higher "repolishing" effect on the same areas that have already experienced the treatment compared to the DoE experiments. The beneficial effect of this second consequence of the beam defocusing could be supported considering that surface finish improvements were observed in a similar experimental work reported elsewhere [45], for which wrought aluminum surfaces were successfully polished with CO2 lasers although having a significantly lower starting roughness compared to the ones observed in this work. Moreover, when the focus position is set closer to the surface, the provided energy distribution on the surface is more localized, resulting in a somewhat higher thermal gradient region and therefore rough surface region.

In conclusion of the surface texture evolution analysis, it is worth to highlight that the investigated process led to an Sa reduction of the 85% considering the best case of the entire experimental campaign. This result is very good in comparison with similar reported works in literature about laser polishing [25,26,46].

4.2. Microstructure evolution

On the macroscale, after laser polishing new molten pools defining the re-melting zone are evident, whose inner microstructure was heterogeneous. Another notable experimental outcome observed in relation to the defocused beam experiments was the increasing presence of porosity as a function of the laser focus shift (see Fig. 11). As well known, those defects are detrimental for the mechanical properties of the processed surface. According to [47], the observed defects are compatible with hydrogen evolution within the molten pool, whose formation may take place following different mechanisms such as moisture absorption from the environment and coalescence from oxides and pores already present in the L-PBF processed material. This result might be ascribed also to the decay of the shielding effect promoted by the argon used in the experiments, as the laser head is further from the free surface. Moreover, according to the effects of the beam defocusing on the OV% discussed in the previous section, an increased residence time of the beam on the same surface region would be expected to have increased the local temperature of the molten pool, thus allowing for increased hydrogen solubility within the processed material. On the other hand, any significant influence of porosities already presents in the L-PBF as-built samples cannot be excluded considering that their presence in the near-surface region was observed (see Fig. 6). Therefore, given the

Manuscript version: Accepted 8 May 2021
Elsevier, Surface & Coatings Technology
https://doi.org/10.1016/j.surfcoat.2021.127291
preliminary experiments conducted in this work and primary aim to optimize the surface quality, the mitigation of those defects needs further investigation.

Table 6
Comparison between the values of the laser spot, E and OV% imposed for DoE best case (Run 10) and the theoretical values calculated for the defocused beam experiments.

	Laser spot (μm)	E (J/mm^2)	OV%
Run 10 (z = 0)	200	330	80
Run 10 F + 1 (z = 1 mm)	210.6	314	80,5
Run 10 F + 2 (z = 2 mm)	240.8	274	83
Run 10 F + 3 (z = 3 mm)	284	232	85

From the SEM microstructure analysis, the results observed from the best cases of both of the presented experimental campaigns (see Figs. 7, 12) showed that the laser polishing promoted a grain coarsening in the PZ. This result, according to the respective OV% values considered, is in agreement with the previous observations based on the optical macrographs and the surface texture evolution concerning the repeated thermal cycles experienced from the material. This result would lead to a decrease of the surface hardness according to the Hall-Petch law. However, the different Al and Si distribution in the PZ compared to the base material counteracted this effect. Further SEM-EDS analyses were carried out on the different regions of the Run 10 F + 3 sample illustrated in Fig. 12. According to the results reported in the Table 7, the microstructure alteration induced during polishing promoted a decrease of the Si content of about 1.5% wt in the HAZ and an increase of about the 0.8% wt in the PZ, compared to the reference chemical composition of the base material. This result, according to exploratory work reported in literature [48], is compatible with an overall increase of the resulting hardness, as confirmed also by Vickers microhardness tests carried out in this work, using a 25 g load applied for a dwell time of 20s. For sake of brevity, the tests were carried out only considering the L-PBF as-built condition, the Run 10 case and the Run 10 F + 3 case. The results, calculated as mean and standard deviation over five indentations for each sample, showed a hardness increase range from 9 to 30% after laser polishing over the as-built condition (As-built: 85 ± 5.4 HV, Run 10: 93 ± 10.3 HV, Run 10 F + 3: 121 ± 12.6 HV). This result suggests therefore an increase of the superficial mechanical properties after CO2 laser polishing.

Table 7
Chemical composition comparison between the different microstructure regions of the Run 10 F + 3 sample, evaluated by means of EDS analysis (Magnification. 5000×).

Element	BM		HAZ		PZ	
	Wt%	Wt% σ	Wt%	Wt% σ	Wt%	Wt% σ
Magnesium	0.462	0.034	0.444	0.034	0.446	0.036
Aluminum	86.385	0.117	87.91	0.115	85.602	0.124
Silicon	13.154	0.114	11.646	0.111	13.952	0.121

It is also worth to mention that the measured differences in chemical composition between the HAZ and the PZ, but more specifically the Si increase in the PZ that promoted the hardness increase, could have also reduced the sensitivity of the molten material to the detrimental

Manuscript version: Accepted 8 May 2021
Elsevier, Surface & Coatings Technology
https://doi.org/10.1016/j.surfcoat.2021.127291
balling effect during laser polishing, thus promoting a flatter surface. According to an experimental work reported in literature concerning the surface tension of Al–Si alloys at elevated temperatures [49], the surface tension decreases when the Si content in the alloy increases. From the point of view of laser polishing, this aspect implicates an enhanced re-melting effect and the inhibition of any balling tendency given the reduced surface tension of the molten pool. Moreover, given that the surface tension decreases also with the temperature increase, the beneficial effect of the laser defocusing on the surface quality is more strongly proved since the focus shift above the surface induced an increase of laser residence time on a fixed surface region and, therefore, a raise of the melt temperature.

5. Conclusions

In this work, a preliminary experimental study was carried out to assess the possibility to use CO2 lasers to perform a surface polishing treatment on AlSi10Mg alloy samples manufactured via L-PBF. To the best knowledge of the authors, this represents the first study conducted in this specific context. The experimental campaign examined how the high surface roughness of the L-PBF processed alloy could be laser polished effectively with a CO2 laser, therefore, extending their use and providing a further useful laser polishing option. In the presented experiments, the effects of laser power, scanning speed, overlap between the polishing tracks and focus position were investigated. Moreover, different surface texture indicators were analyzed for a better understanding of the process mechanisms, whose discussion was also supported with a detailed microstructure analysis and microhardness measurements. According to the results obtained, the following conclusions can be drawn:

- Considering an average Sa value of 21.5 μm for the as-built samples and a wavelength value of 10.6 μm for the laser surface polishing implemented, a resulting Sa/λ ratio of 2 was examined. The set-up implemented proved to be effective in order to perform laser polishing;
- According to the results obtained from the DoE experiments and the related process parameter window, a combined increase of the areal energy density (E) and the percentage overlap between the tracks (OV%) promoted a significant surface quality improvement. In this context, an energy density value of 330 J/mm2 (obtained from a laser power of 550 W and a scanning speed of 500 mm/min) and an OV% value of 80% promoted an Sa decrease of 65%;
- The surface roughness (Sa) reduction was increased to 85% when the previously mentioned process parameters were adopted in combination with a laser focus position of 3 mm above the surface peaks. This result is in line with the most results observed for the case of laser polishing with fibre laser;
- The evolution of the surface skewness (Ssk) towards values close to zero suggested a more symmetrical surface after the best polishing condition for the entire experimental campaign;
- The evolution of the primary profile slope (Pdq) suggested a similar dependency as Sa with respect to the controlled process parameters. However, laser focus position did not affect significantly this parameter, despite the further Sa decrease for the defocused beam polishing condition. This result indicated that a primary polishing mechanism of the considered surfaces is the removal of the aforementioned sintered powders by means of surface re-melting, leading to a 90% decrease in Pdq for the best case of the entire experimental campaign;

- The laser polishing process induced a coarser microstructure within the re-molten layer with respect to the bulk material. However, the microhardness of the laser polished material experienced an increase of the 9% for the best DoE case and the 30% for the best defocused beam condition with respect to the 85 HV value of the as-built condition. This result was justified by a Si content increase of about 0.8 wt% in the re-molten zone, subsequent to a re-distribution from the HAZ.

CRediT authorship contribution statement

Andrea El Hassanin: Conceptualization, Methodology, Visualiza tion, Investigation, Data curation, Writing- Original draft preparation, Writing - Review & Editing.

Muhannad Ahmed Obeidi: Conceptualization, Methodology, Data curation, Visualization, Investigation, Writing - Review & Editing.

Fabio Scherillo: Methodology, Data curation, Visualization, Investigation, Writing - Review & Editing.

Dermot Brabazon: Conceptualization, Visualization, Data curation, Writing - Review & Editing, Resources, Funding acquisition, Supervision.

Declaration of competing interest

The authors declare that they have no known competing financial interests or personal relationships that could have appeared to influence the work reported in this paper.

Acknowledgments

work was carried out within a mobility research program between the University of Naples Federico II and the Dublin City University (DCU), supported by the Mobility Grant for Ph.D. students provided from the International Conference on Material Forming (ESAFORM). Therefore, the authors would like to thank ESAFORM for supporting the activity by the provided funding. The authors would like to acknowledge the support from the Science Foundation Ireland (SFI) research grant number 16/RC/3872 and co-funding under the European Regional Development Fund.

References

[1] I. Gibson, D.W. Rosen, B. Stucker, Additive Manufacturing Technologies, Springer Verlag, New York, 2015.
[2] W.E. Frazier, Metal additive manufacturing: a review, J. Mater. Eng. Perform. 23 (2014) 1917–1928, https://doi.org/10.1007/s11665-014-0958-z.
[3] T. DebRoy, H.L. Wei, J.S. Zuback, T. Mukherjee, J.W. Elmer, J.O. Milewski, A. M. Beese, A. Wilson-Heid, A. De, W. Zhang, Additive manufacturing of metallic components – process, structure and properties, Prog, Mater. Sci. 92 (2018) 112–224, https://doi.org/10.1016/j.pmatsci.2017.10.001.
[4] F. Cabanettes, A. Joubert, G. Chardon, V. Dumas, J. Rech, C. Grosjean, Z. Dimkovski, Topography of as built surfaces generated in metal additive

manufacturing: a multi scale analysis from form to roughness, Precis, Eng. 52 (2018) 249–265, https://doi.org/10.1016/j.precisioneng.2018.01.002.
[5] N. Sanaei, A. Fatemi, Analysis of the effect of surface roughness on fatigue performance of powder bed fusion additive manufactured metals, Theor. Appl. Fract. Mech. 108 (2020), 102638, https://doi.org/10.1016/j.tafmec.2020.102638.
[6] G. Strano, L. Hao, R.M. Everson, K.E. Evans, Surface roughness analysis, modelling and prediction in selective laser melting, J. Mater. Process. Technol. 213 (2013) 589–597, https://doi.org/10.1016/j.jmatprotec.2012.11.011.
[7] E. Beevers, A.D. Brandˇ
ao, J. Gumpinger, M. Gschweitl, C. Seyfert, P. Hofbauer,
T. Rohr, T. Ghidini, Fatigue properties and material characteristics of additively manufactured AlSi10Mg – effect of the contour parameter on the microstructure, density, residual stress, roughness and mechanical properties, Int. J. Fatigue 117 (2018) 148–162, https://doi.org/10.1016/j.ijfatigue.2018.08.023.
[8] E. Maleki, S. Bagherifard, M. Bandini, M. Guagliano, Surface post-treatments for metal additive manufacturing: progress, challenges, and opportunities, Addit. Manuf. (2020), 101619, https://doi.org/10.1016/j.addma.2020.101619.
[9] J.Y. Lee, A.P. Nagalingam, S.H. Yeo, A review on the state-of-the-art of surface finishing processes and related ISO/ASTM standards for metal additive manufactured components, Virtual Phys. Prototyp. (2020), https://doi.org/10.1080/17452759.2020.1830346.
[10] J.M. Flynn, A. Shokrani, S.T. Newman, V. Dhokia, Hybrid additive and subtractive machine tools - research and industrial developments, Int. J. Mach. Tools Manuf. 101 (2016) 79–101, https://doi.org/10.1016/j.ijmachtools.2015.11.007.
[11] Y. Kaynak, O. Kitay, The effect of post-processing operations on surface characteristics of 316L stainless steel produced by selective laser melting, Addit. Manuf. 26 (2019) 84–93, https://doi.org/10.1016/j.addma.2018.12.021.
[12] B. AlMangour, J.M. Yang, Improving the surface quality and mechanical properties by shot-peening of 17-4 stainless steel fabricated by additive manufacturing, Mater. Des. 110 (2016) 914–924, https://doi.org/10.1016/j.matdes.2016.08.037.
[13] A. Maamoun, M. Elbestawi, S. Veldhuis, Influence of shot peening on AlSi10Mg parts fabricated by additive manufacturing, J. Manuf. Mater. Process. 2 (2018) 40, https://doi.org/10.3390/jmmp2030040.
[14] M.A. Bernevig-Sava, C. Stamate, N.M. Lohan, A.M. Baciu, I. Postolache, C. Baciu, E. R. Baciu, Considerations on the surface roughness of SLM processed metal parts and the effects of subsequent sandblasting, IOP Conf, Ser. Mater. Sci. Eng. 572 (2019), https://doi.org/10.1088/1757-899X/572/1/012071.
[15] J. Gumpinger, A.D. Brandao, E. Beevers, T. Rohr, T. Ghidini, S. Beretta, S. Romano, Expression of additive manufacturing surface irregularities through a flaw-based assessment, Rev. ASTM Sel. Tech. Pap. (2019).
[16] E. Atzeni, M. Barletta, F. Calignano, L. Iuliano, G. Rubino, V. Tagliaferri, Abrasive Fluidized Bed (AFB) finishing of AlSi10Mg substrates manufactured by Direct Metal Laser Sintering (DMLS), Addit. Manuf. 10 (2016) 15–23, https://doi.org/10.1016/j.addma.2016.01.005.
[17] A. El Hassanin, M. Troiano, A.T. Silvestri, V. Contaldi, F. Scherillo, R. Solimene, F. Scala, A. Squillace, P. Salatino, Fluidised bed machining of metal additive manufactured parts, in: AIP Conf. Proc. 2113, 2019, https://doi.org/10.1063/1.5112685.
[18] A. El Hassanin, M. Troiano, F. Scherillo, A.T. Silvestri, V. Contaldi, R. Solimene, F. Scala, A. Squillace, P. Salatino, Rotation-assisted abrasive fluidised bed

machining of alsi10mg parts made through selective laser melting technology, Procedia Manuf. 47 (2020) 1043–1049, https://doi.org/10.1016/j.promfg.2020.04.113.
[19] A.P. Nagalingam, H.K. Yuvaraj, S.H. Yeo, Synergistic effects in hydrodynamic cavitation abrasive finishing for internal surface-finish enhancement of additive manufactured components, Addit. Manuf. 33 (2020), 101110, https://doi.org/10.1016/j.addma.2020.101110.
[20] U.S. Kim, J.W. Park, High-quality surface finishing of industrial three-dimensional metal additive manufacturing using electrochemical polishing, Int. J. Precis. Eng. Manuf. - Green Technol. 6 (2019) 11–21, https://doi.org/10.1007/s40684-019-00019-2.
[21] P. Tyagi, T. Goulet, C. Riso, F. Garcia-Moreno, Reducing surface roughness by chemical polishing of additively manufactured 3D printed 316 stainless steel components, Int. J. Adv. Manuf. Technol. 100 (2019) 2895–2900, https://doi.org/10.1007/s00170-018-2890-0.
[22] F. Scherillo, Chemical surface finishing of AlSi10Mg components made by additive manufacturing, Manuf, Lett. 19 (2019) 5–9, https://doi.org/10.1016/j.mfglet.2018.12.002.
[23] E. Lyczkowska, P. Szymczyk, B. Dybała, E. Chlebus, Chemical polishing of scaffolds made of Ti-6Al-7Nb alloy by additive manufacturing, Arch, Civ. Mech. Eng. 14 (2014) 586–594, https://doi.org/10.1016/j.acme.2014.03.001.
[24] R. Poprawe, Tailored Light 2 Laser Application Technology, Springer, Berlin Heidelberg, Aachen, 2011.
[25] B. Liu, B.Q. Li, Z. Li, Selective laser remelting of an additive layer manufacturing process on AlSi10Mg, Results Phys. 12 (2019) 982–988, https://doi.org/10.1016/j.rinp.2018.12.018.
[26] Q. Han, Y. Jiao, Effect of heat treatment and laser surface remelting on AlSi10Mg alloy fabricated by selective laser melting, Int. J. Adv. Manuf. Technol. 102 (2019) 3315–3324, https://doi.org/10.1007/s00170-018-03272-y.
[27] B. Rosa, P. Mognol, J. Hasco¨et, B. Rosa, P. Mognol, J.H. Laser, P. Mognol, J. Y. Hascoet, Laser polishing of additive laser manufacturing surfaces to cite this version : HAL Id : hal-01149709, 2015.
[28] M.A. Obeidi, E. Mccarthy, I.U. Ahad, Laser Polishing of Additive Manufactured 316L SST Cylindrical Samples, (n.d.).
[29] J. Li, D. Zuo, Laser polishing of additive manufactured Ti6Al4V alloy: a review, Opt. Eng. 60 (2021) 1–16, https://doi.org/10.1117/1.oe.60.2.020901.
[30] D. Bourell, J.P. Kruth, M. Leu, G. Levy, D. Rosen, A.M. Beese, A. Clare, Materials for additive manufacturing, CIRP Ann. - Manuf. Technol. 66 (2017) 659–681, https://doi.org/10.1016/j.cirp.2017.05.009.
[31] A. Sassmannshausen, A. Brenner, J. Finger, Ultrashort pulse laser polishing by continuous surface melting, J. Mater. Process. Technol. 293 (2021), 117058, https://doi.org/10.1016/j.jmatprotec.2021.117058.
[32] O. El-Mowafy, N. El-Aawar, N. El-Mowafy, A. Pahlevan, M. Mirzaee, E. Yassine, L. Ranjbar Omrany, M. Hasani Tabatabaee, H. Kermanshah, S. Arami, M. Abbasi, C. F. Driscoll, M.A. Freilich, A.D. Guckes, K.L. Knoernschild, T.J. Mcgarry, G. Goldstein, C. Goodacre, A.D. Guckes, S. Mor, S. Rosenstiel, C. Vanblarcom, Y. F. Mak, S.C.N. Lai, G.S.P. Cheung, A.W.K. Chan, F.R. Tay, D.H. Pashley, M. O. Oztoprak, M. Tozlu, U. Iseri, F. Ulkur, T. Arun, M.L. Gurney, S.D. Sharples, W. B. Phillips, D.J. Lee, A. Perveen, C. Molardi, C. Fornaini, F. Sanz, J.A. Manzanares, A. Kumar, N.S. Bandeshah, A. Nanda, R.K. Bandeshah, C. Gupta, State of the art of

CO2 laser beam machining, Micromachines. 18 (2018) 90–94, https://doi.org/10.17219/dmp/90729.
[33] M.A. Obeidi, E. McCarthy, L. Kailas, D. Brabazon, Laser surface texturing of stainless steel 316L cylindrical pins for interference fit applications, J. Mater. Process. Technol. 252 (2018) 58–68, https://doi.org/10.1016/j.jmatprotec.2017.09.016.
[34] M.A. Obeidi, E. McCarthy, D. Brabazon, Methodology of laser processing for precise control of surface micro-topology, Surf, Coatings Technol. 307 (2016) 702–712, https://doi.org/10.1016/j.surfcoat.2016.09.075.
[35] https://www.rofin.com/fileadmin/user_upload/biografien/COHR_DC_Series_DS_0619web.pdf. [accessed in 10 January 2021].
[36] S.M. Thompson, L. Bian, N. Shamsaei, A. Yadollahi, An overview of direct laser deposition for additive manufacturing; part I: transport phenomena, modeling and diagnostics, Addit. Manuf. 8 (2015) 36–62, https://doi.org/10.1016/j.addma.2015.07.001.
[37] J.C. Ion, Laser Processing of Engineering Materials — Principles, Procedure and Industrial Application, first ed. Butterworth-Heinemann, Cambridge, 2005.
[38] A. Townsend, N. Senin, L. Blunt, R.K. Leach, J.S. Taylor, Surface texture metrology for metal additive manufacturing: a review, Precis, Eng. 46 (2016) 34–47, https://doi.org/10.1016/j.precisioneng.2016.06.001.
[39] ISO25178-2, BSI Standards Publication Geometrical Product Specifications (GPS) — Surface Texture : Areal Part 2 : Terms , Definitions and Surface, (2012).
[40] ISO4287, BSI Standards Publication Geometrical Product Specifications (GPS) — Surface Texture: Profile Method: Terms, Definitions and Surface Texture Parameters, British Standards Institution, 1998.
[41] https://www.olympus-ims.com/it/metrology/surface-roughness-measurement-portal/parameters/#!cms[focus]=cmsContent14708&cms[tab]=undefined [accessed in 7 December 2020].
[42] M. Yonehara, T. Matsui, K. Kihara, H. Isono, A. Kijima, T. Sugibayashi, Evaluation method of surface texture by surface roughness based on geometrical product specifications (GPS), Mater. Trans. 45 (2004) 1019–1026, https://doi.org/10.2320/matertrans.45.1019.
[43] K. Geels, D.B. Fowler, W.U. Kopp, M. Rückert, Metallographic and Materialographic Specimen Preparation Light Microscopy Image Analysis and Hardness Testing, ASTM International, Lancaster, 2007.
[44] L.P. Lam, D.Q. Zhang, Z.H. Liu, C.K. Chua, Phase analysis and microstructure characterisation of AlSi10Mg parts produced by selective laser melting, Virtual Phys. Prototyp. 10 (2015) 207–215, https://doi.org/10.1080/17452759.2015.1110868.
[45] M.A. Obeidi, E. McCarthy, S.I. Ubani, I. Ul Ahad, D. Brabazon, Effect of surface roughness on CO2 laser absorption by 316L stainless steel and aluminum, Mater. Perform. Charact. 8 (2019), 20180091, https://doi.org/10.1520/mpc20180091.
[46] J. Schanz, M. Hofele, S. Ruck, T. Schubert, L. Hitzler, G. Schneider, M. Merkel, H. Riegel, Metallurgical investigations of laser remelted additively manufactured AlSi10Mg parts: Metallurgische Untersuchungen von laserstrahlumgeschmolzenen additiv hergestellten AlSi10Mg Bauteilen, Materwiss, Werksttech. 48 (2017) 463–476, https://doi.org/10.1002/mawe.201700039.
[47] X. Cao, W. Wallace, J.P. Immarigeon, C. Poon, Research and progress in laser welding of wrought aluminum alloys, II. Metallurgical microstructures, defects, and mechanical properties, Mater. Manuf. Process. 18 (2003) 23–49, https://doi.

Manuscript version: Accepted 8 May 2021
Elsevier, Surface & Coatings Technology
https://doi.org/10.1016/j.surfcoat.2021.127291
org/10.1081/AMP-120017587.
[48] A. Mertens, J. Delahaye, O. Dedry, B. Vertruyen, J.T. Tchuindjang, A.M. Habraken, Microstructure and properties of SLM AlSi10Mg: understanding the influence of the local thermal history, Procedia Manuf. 47 (2020) 1089–1095, https://doi.org/10.1016/j.promfg.2020.04.121.
[49] L. Dou, Z.F. Yuan, J.Q. Li, J. Li, X.Q. Wang, Surface tension of molten Al-Si alloy at temperatures ranging from 923 to 1123 K, Chinese Sci, Bull. 53 (2008) 2593–2598, https://doi.org/10.1007/s11434-008-0372-8.